Available online at www.sciencedirect.com
ScienceDirect
Combustion and Flame 151 (2007) 532–541
Combustion and Flame
www.elsevier.com/locate/combustflame

The effect of strain rate on polycyclic aromatic hydrocarbon (PAH) formation in acetylene diffusion flames

Manabu Yamamoto, Shici Duan, Selim Senkan *

Department of Chemical Engineering, University of California, Los Angeles, CA 90095, USA

Received 15 February 2005; received in revised form 30 April 2006; accepted 15 May 2006

Available online 5 September 2007

Abstract

Acetylene is a ubiquitous combustion intermediate that is also believed to be the major precursor for aromatic, polycyclic aromatic hydrocarbon (PAH), and soot formation in both hydrocarbon and halogenated hydrocarbon flames. However, in spite of its important role as a flame intermediate, the detailed chemical structures of acetylene diffusion flames have not been studied in the past. Here the detailed chemical structures of counterflow diffusion flames of acetylene at strain rates of 37.7 and 50.3 s^{-1} are presented. Both flames possessed the same carbon density of 0.37 g/L corresponding to an acetylene mole fraction of 0.375 in argon on the fuel side, and an oxygen mole fraction of 0.22 in argon on the oxidizer side. Concentration profiles of a large number of major, minor, and trace species, including a wide spectrum of aromatics and PAH, have been determined by direct sampling from flames using a heated quartz microprobe coupled to an online gas chromatograph/mass selective detector (GC/MSD). Temperature profiles were made using a thermocouple and the rapid insertion technique. Although the major species concentrations were nearly the same in the two flames, the mole fraction profiles of trace combustion by-products were significantly lower in the higher-strain-rate flame, by nearly two orders of magnitude for PAH. These comparative results provide new information on the trace chemistries of acetylene flames and should be useful for the development and validation of detailed chemical kinetic mechanisms describing the formation of toxic by-products in the combustion of hydrocarbons and halogenated hydrocarbons.

Keywords: Air toxins; Soot precursors; Combustion by-products; Counterflow; Acetylene; Diffusion flames

1. Introduction

Acetylene is one of the most abundant intermediates in hydrocarbon combustion (see, for example, [3,12] and references therein) as well as in the combustion of halogenated hydrocarbons such as CH_3Br [4] and CH_2Cl_2 [5]. Acetylene is also believed to be an important precursor for the formation of polycyclic aromatic hydrocarbons (PAH) and soot [6–8]. Since some PAH isomers (such as benzo-a-pyrene), as well as their halogenated aromatics (such as dioxins and furans), are potentially toxic, it is important to develop combustion strategies that minimize their emission from combustion systems. One way to achieve this goal is through the use of predictive, model-based control systems for the operation of combustors and waste incinerators. To develop model-based control systems, mathematical models describing both the transport (i.e., momentum, heat,

* Corresponding author.
E-mail address: senkan@ucla.edu (S. Senkan).

0010-2180/$ – see front matter
doi:10.1016/j.combustflame.2006.06.001

and mass transfer) and the chemical kinetics of fuel destruction must be developed. Transport models describing specific combustion equipment have successfully been developed and used to describe some of the general performance characteristics of combustion devices (see, for example, [9,10] and references therein). On the other hand, detailed quantitative chemical kinetic mechanisms describing combustion reaction processes, including the formation and emission of trace pollutants such as PAH and dioxins, still need to be developed and validated.

One-dimensional laminar premixed flames and axisymmetric opposed jet diffusion flames have successfully been used to gain useful insights into the detailed chemical kinetics of combustion through the acquisition of detailed species concentration profiles. The one-dimensional and laminar nature of these laboratory flames enables the accurate modeling of the underlying transport phenomena, thereby rendering the model predictions particularly sensitive to the detailed chemical kinetic mechanism used in the simulation process [7,8,11,12].

Counterflow diffusion flames represent a particularly relevant and useful framework for studying combustion chemistry for several reasons. First, they mimic practical combustion systems where the fuel and air are not mixed prior to the flame zone, thus allowing the simulation of fuel pyrolysis and PAH formation in the oxygen-starved regions of combustors. Second, counterflow diffusion flames also have a central axis of symmetry, which allows the reduction of their two-dimensionality into one-dimensionality by the introduction of a stream function for the solution of mass, momentum, and energy balances.

Previous studies in counterflow diffusion flames focused primarily on NO_x formation [13,14], flame extinction [15,16], major species [17], and soot formation [18,19]. Only recently have systematic studies regarding the detailed structures of counterflow diffusion flames of hydrocarbon fuels been undertaken [1,3,20,21].

Acetylene combustion has previously been studied by a number of investigators, primarily in low-pressure premixed flames (see, for example, [22,23]). Detailed chemical kinetic mechanisms of acetylene combustion were also developed [7,23] and partially validated, using the limited data available from low-pressure premixed flames noted above.

Experimental data on the structures of diffusion flames of acetylene are very scarce. Sunderland et al. [19,24] reported studies on soot formation and temperature profiles in a turbulent diffusion flame. Sun et al. [17] measured the temperature and major species concentration profiles in a counterflow diffusion flame of acetylene using the spontaneous Raman scattering technique. Their numerical simulation of the temperature and major species concentration profiles was in reasonable agreement with the experimental results. In addition, they concluded that the dominant C_2H_2 oxidation step for acetylene flames involves the reaction of acetylene with oxygen atoms. We are not aware of any earlier studies where detailed chemical structures of acetylene diffusion flames were ever investigated.

Therefore the objective of this paper is to report on the detailed chemical structures of atmospheric-pressure laminar counterflow diffusion flames of acetylene as a function of strain rate. The effects of carbon density on acetylene flame structure will be reported in the future.

2. Experimental setup

The counterflow burner system and sampling configuration are illustrated in Fig. 1. The acetylene diffusion flames were stabilized between two opposed jet nozzles (ID 2.54 cm). The oxidizer stream, which was 22% O_2 and 78% Ar, was introduced from the upper nozzle. The fuel stream, containing 37.5% C_2H_2 and 62.5% Ar by volume, was introduced from the lower nozzle. All gases used were of high purity (Matheson, Cucamonga, CA). To minimize the trace impurities in acetylene (mostly acetone), a cold trap system was used, as shown in Fig. 1. Three vacuum traps (45 × 350 mm, Chemglass) were connected in series. The entire trap system was then placed in a bath of 2-propanol, which was cooled to −45 °C by bubbling liquid nitrogen or carbon dioxide.

A series of 100 mesh screens were used at the exit of each jet to establish uniform gas flow velocities to generate stable, flat flames. Argon gas was used to shield and protect the flame from the surrounding air. Using a mild vacuum through the holes in the annular section of the bottom burner, combustion products and shield gas were vented out of the system.

A heated quartz microprobe (OD 0.635 cm) with a 125×10^{-4}-cm-diameter orifice at its tip was used to withdraw samples from the center of the flame. The tip was conically tapered at an angle of about 20°. The probe orifice diameter used was the smallest possible size to achieve sampling in sooting flames. Soot particles in the sample were trapped using a heated high-purity silica fiber filter before gas analysis.

Possible systematic errors in species concentration measurements have been examined. The degree of reaction quenching and the possibility of formation of pyrolysis products in the probe were tested by sampling from the flame at different transfer line pressures and temperatures. These measurements indicated that the effects of the probe on flame chemistry were negligible. Furthermore, the possi-

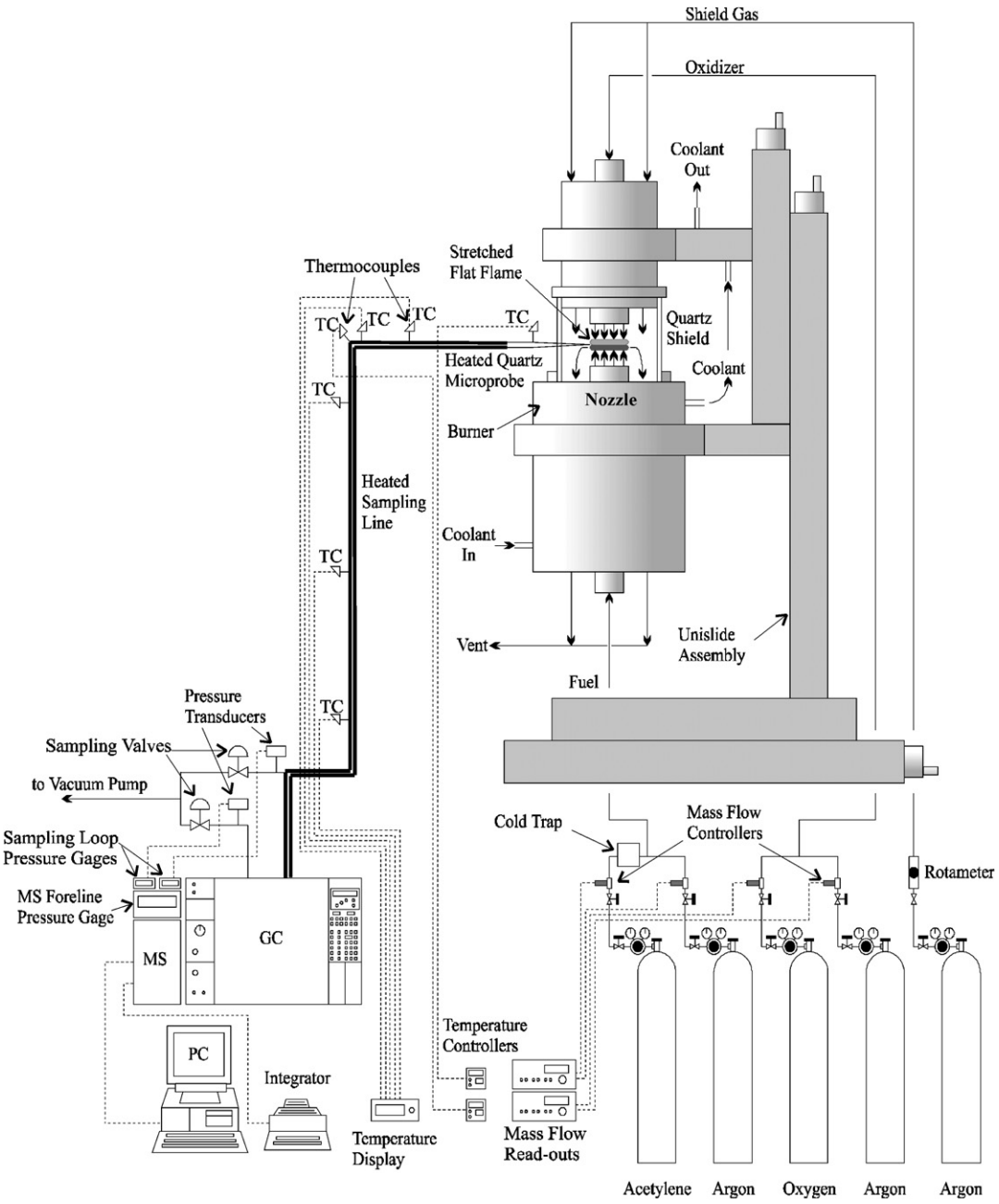

Fig. 1. Experimental setup of counterflow diffusion flame burner.

ble contribution of radical–radical and radical–stable species reactions to measurements of abundant stable species concentrations (e.g., benzene) was also considered [1]. These investigations showed that even if all the radicals were quantitatively converted to their corresponding stable products, their contributions to measured concentrations would be less than 1–5%. The possible catalytic activities of the sampling probe and transfer line surfaces were also explored by varying the temperature; these measurements also did not exhibit any significant variations in measured compositions within the experimental conditions investigated.

Based on vapor pressure considerations, most of the PAH with 252 amu or less should remain in the gas phase at 300 °C and above [25]. Therefore, the sampling system, which includes the probe, soot trap, silica-coated transfer lines, and GC multiport valves,

was kept at about 300 °C to minimize the adsorption of high-molecular-weight PAH on surfaces.

An online microprocessor-controlled gas chromatograph/mass spectrometer (Hewlett–Packard 5890/5971) system was used to analyze the gas samples. Major species were separated using packed columns (Hayesep-T, Hayesep-A, and Molecular Sieve) connected to a thermal conductivity detector having a detection sensitivity of about 10^{-3}–10^{-4} mole fraction, depending on the species. The minor and all trace species were separated by a capillary column (0.32 mm × 60 m HP-5) interfaced to the mass spectrometer detector, which had a sensitivity of measuring species with mole fractions as low as 10^{-8}.

For the light and most of the intermediate-molecular-weight species, a certified gas mixture acquired from Matheson Co. (Cucamonga, CA) was used for calibration. Retention times as well as mass spectral fingerprints matched to standard MS libraries (Wiley Mass Spectral Database, 1991) were used for species identification. Species concentrations were then determined using calibration mixtures. The accuracy of the species mole fractions was estimated to be about 15%. The relative ionization cross-section method was used [26] to quantify species mole fractions whose calibration standards were not available. This method has been tested and shown to be accurate within a factor of 2 in previous studies [2].

Using a high-precision (0.01-mm) translation system, sampling position within the flame was changed by moving the entire burner assembly up or down with respect to the fixed sampling probe and the thermocouple to determine the species and temperature profiles, respectively. Positional accuracy of the concentration and temperature profiles with respect to the burner surface was estimated to be ±0.25 mm.

The temperature measurements were done using a silica-coated Pt/Pt + 13%Rh (R type, Omega) thermocouple with 0.075-mm wire and a bead diameter of about 0.200 mm. A rapid insertion technique was applied to obtain the temperature profiles [27]. To minimize the heat conduction along the wires, the thermocouple was positioned parallel to the burner surface. The soot that was deposited on the thermocouple while probing in the sooting region was burnt off by using a propane torch. The surface of the thermocouple was visually inspected to ensure that it was clean and ready for the next insertion. Flame temperature profiles were acquired automatically using computer-controlled (LABVIEW, National Instruments, Version 5.0.1) stepper-motor-driven linear stages (Velmex Inc., Model No. M062-LS09). A Data Translation A/D board (ADAC, American Data Acquisition Comp., Model 5508-SCI-0-0-3) was used to acquire and digitize analog inputs. Details of the rapid insertion experimental setup can be found elsewhere [28]. Here, direct thermocouple junction readings without any radiation corrections are reported.

3. Results and discussion

Experimental conditions investigated are given in Table 1. These conditions were determined to provide stable, laminar, flat flames after extensive preliminary studies. The flames exhibited three visually distinct zones; the blue zone at the oxidizer side, together with the luminous yellow and orange zones located just below the blue zones. All concentration and temperature profiles were measured at the center of the flame ($r = 0$) to minimize the edge effects.

Strain rate is one of the most important flame parameters that influence the structure of counterflow diffusion flames. A strain (or stretch) occurs on a flame surface due to the velocity gradient in the axial direction. Higher strain rates induce thinner flames and lower flame temperatures because of shorter residence times for the reactants in the combustion zone, which decreases the extent of chemical reaction. The further increase of strain rate will ultimately result in flame extinction. The strain rate can be calculated with the following equation derived by Seshadri and Williams [29],

$$K = -\frac{2V_0}{L}\left[1 + \frac{V_f}{V_0}\left(\frac{\rho_f}{\rho_0}\right)^{1/2}\right] (\mathrm{s}^{-1}),$$

where K is the strain rate and L, V_f, V_0, ρ_f, and ρ_0 are the burner separation distance, fuel outlet velocity, oxidizer outlet velocity, fuel density, and oxidizer density, respectively. Although it is well known that the local strain rate in the flame is different from a global definition above, K values were used as a parameter in order to make comparisons between the flames studied.

In the present experiments, flames with overall strain rates of 37.7 and 50.3 s^{-1} were explored, and they are identified as S38 and S50, respectively. The changes in the strain rate were obtained by simultaneously changing the fuel- and oxidizer-side gas flow rates. That is, neither the burner port separation distance nor the gas densities were changed.

Carbon density of a fuel stream is also important in controlling the identities and relative concentrations of the fuel breakdown products. Carbon density is defined by the expression

$$\rho_C = \frac{P}{RT} X_f N_C M_C,$$

where ρ_C, P, R, T, X_f, N_C, and M_C are the carbon density, stream pressure, gas constant, stream temperature, mole fraction, number of carbons in one

Table 1
Experimental conditions for different strain rates

	Symbol	S38	S50
Strain rate, s^{-1}	K	37.7	50.3
Overall equivalence ratio	ϕ	2.05	
Fuel side carbon density, g/L	ρ_C	0.37	
Acetylene mole fraction	X_f	0.375	
Oxidizer mole fraction	X_0	0.220	
Fuel port outlet velocity, mm/s	V_f	131.6	175.5
Oxidizer port outlet velocity, mm/s	V_0	164.5	219.4
Fuel port inlet stream density, g/L	ρ_f	1.42	
Oxidizer port inlet stream density, g/L	ρ_0	1.56	
Fuel and oxidizer inlet temperature, °C	T	25.0	
Burner separation distance, mm	L	15.4	

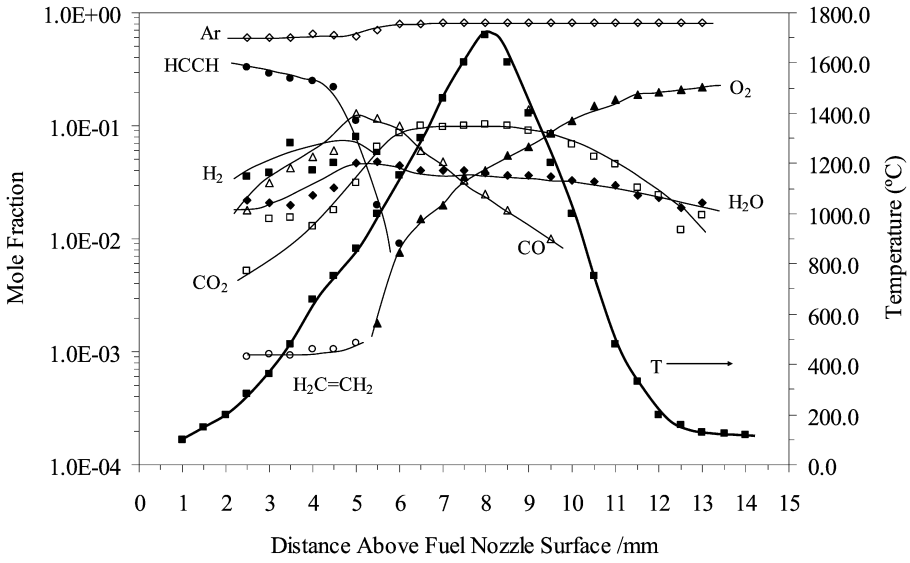

Fig. 2. Profiles of major species mole fractions and temperature for the S38 flame.

molecule of fuel (for acetylene, $N_C = 2$), and carbon atomic weight ($M_C = 12.011$). In the present experiments, the fuel-side carbon density was kept at 0.37 g/L, corresponding to 37.5% by volume of acetylene in argon.

The temperature and major species mole fraction profiles, which include hydrogen (H_2), water (H_2O), acetylene (C_2H_2), carbon monoxide (CO), ethylene (C_2H_4), O_2, Ar, and carbon dioxide (CO_2), are presented in Fig. 2 for the low-strain flame S38. In this and subsequent figures, lines were drawn through the data points to show the experimental trends. Similar profiles for the higher strain rate flame, i.e., the S50 flame, are shown in Fig. 3.

As seen in Fig. 2, a maximum flame temperature of 1700 °C (uncorrected) was reached in the S38 flame at 7.5 mm above the fuel burner surface. The C_2H_2 mole fraction profile shows a gradual decrease until 4.5 mm and decreases sharply thereafter, reaching nondetect levels after 6.0 mm. The O_2 mole fraction profile, on the other hand, exhibits a gradual decrease toward the fuel burner, reaching nondetect levels below 5.5 mm. The maximum mole fractions of complete combustion products CO_2 and H_2O were measured to be 0.1 and 0.05 at 6.0 and 8.0 mm from the fuel burner surface, respectively. The mole fractions of partial combustion products CO and H_2 peaked early in the fuel zone, about 4.0–5.0 mm from the fuel burner port, reaching levels 0.1 and 0.07, respectively.

Similarly, the temperature and major species mole fraction profiles for the higher strain rate S50 flame are presented in Fig. 3. Although qualitatively the profiles for both flames appear similar, there were significant differences. To better illustrate these differences, mole fraction profiles of select species for both the S38 and S50 flames will be presented together for the remainder of the paper. Mole fraction profiles for

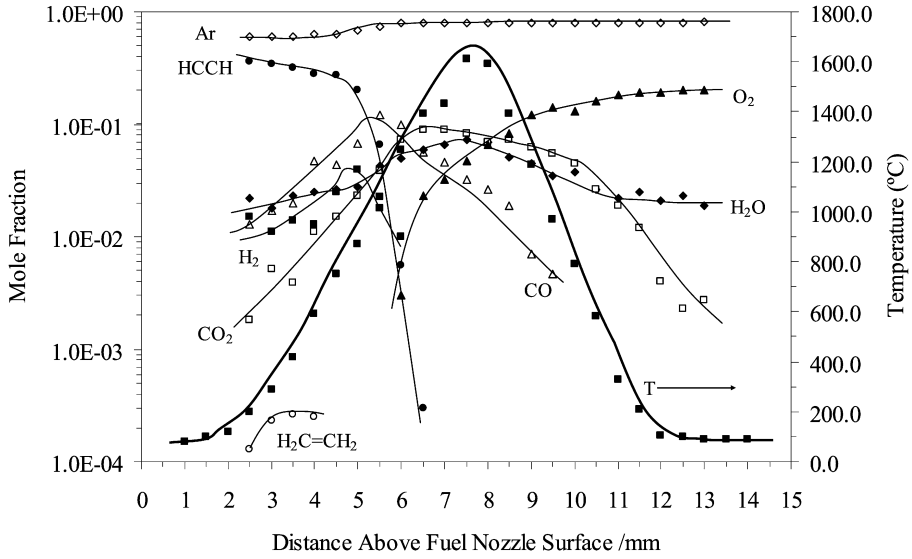

Fig. 3. Profiles of major species mole fractions and temperature for the S50 flame.

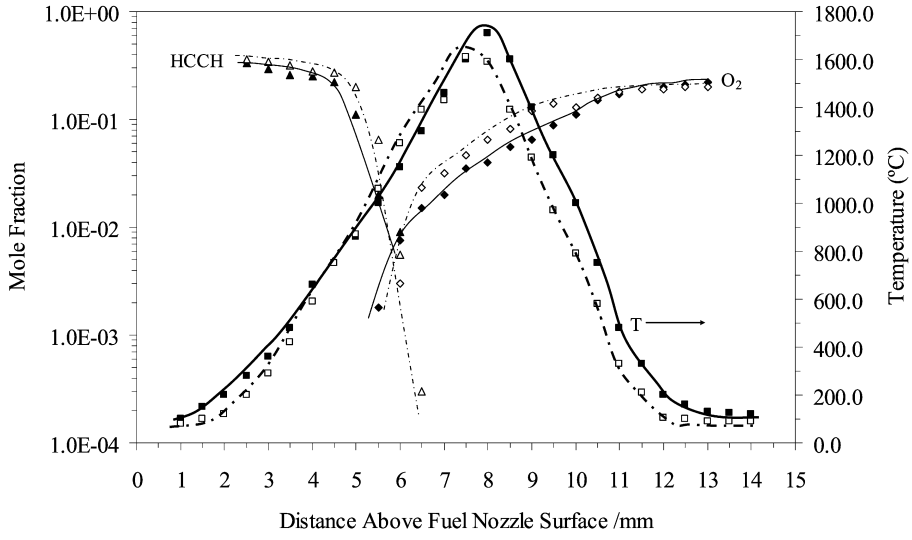

Fig. 4. Profiles of reactant mole fractions and temperature for the S38 (closed symbols, —) and S50 (open symbols, – · –) flames.

the all the species measured in both flames (over 30 species) can be found in Yamamoto [30].

In Fig. 4 the temperature and reactant species mole fraction profiles for both flames are shown. As can be seen clearly from this figure, increasing strain rate decreased the peak flame temperature from 1700 to 1600 °C, as well as shifting the location of this peak toward the fuel side, i.e., closer to the stagnation plane. Higher strain rate also resulted in the establishment of a narrower reaction zone, concomitant with a more abrupt decay in the mole fractions of the fuel and the oxidant as the fuel extinction point is reached. In Figs. 5 and 6, comparisons of the CO_2 and H_2O and the H_2 and CO mole fraction profiles are presented, respectively. The peak mole fractions and locations of CO for the S38 and the S50 flames were 0.12 at 5.0 mm and 0.11 at 5.5 mm, respectively. The peak mole fractions and locations for H_2 were 0.07 at 5.0 mm and 0.04 at 5.0 mm for the S38 and S50 flames, respectively. An inspection of the results presented in Figs. 4–6 reveals that the qualitative and to a lesser degree the quantitative features of the S38 and S50 flames were similar with regard to major species concentration profiles. In addition, these profiles show the characteristics of a typical diffusion flame [1], and as such are consistent with the follow-

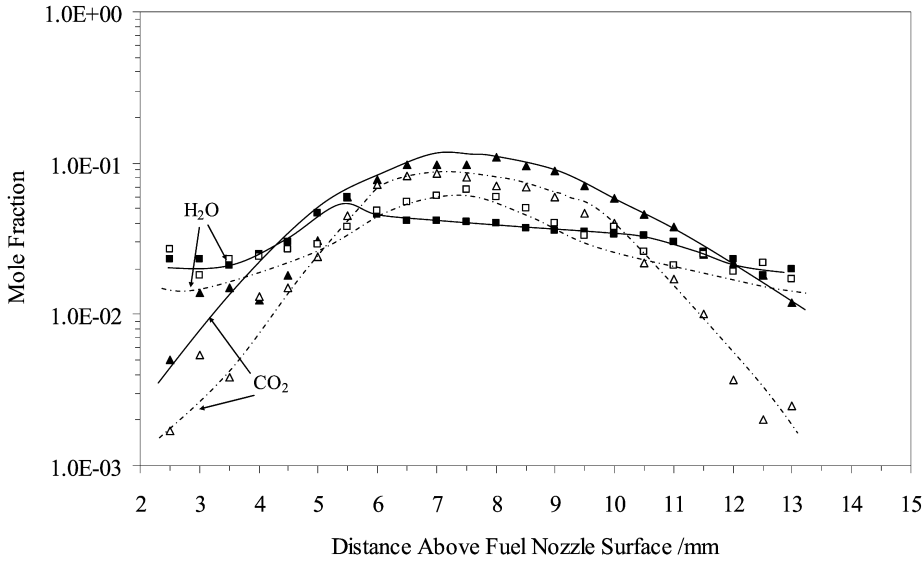

Fig. 5. Mole fraction profiles of complete combustion products for the S38 (closed symbols, —) and S50 (open symbols, – · –) flames.

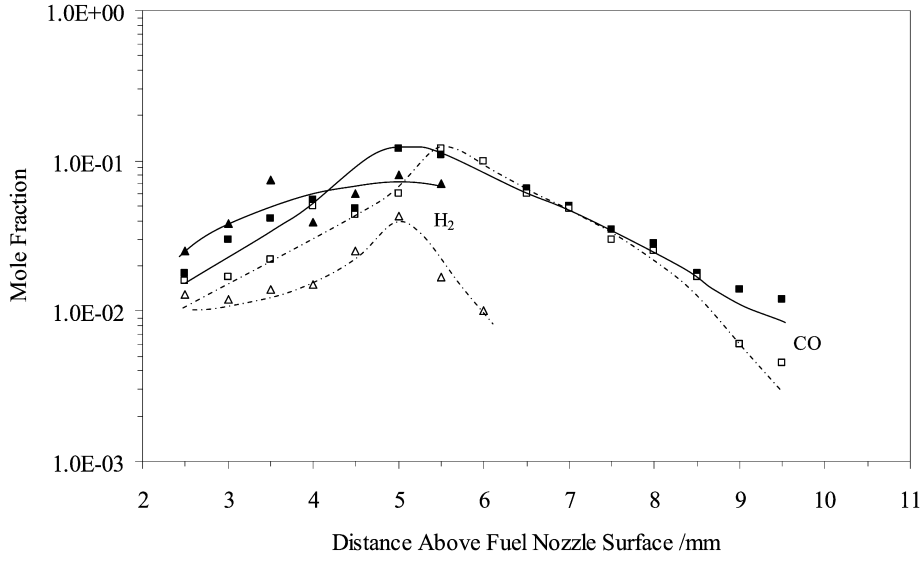

Fig. 6. Mole fraction profiles of incomplete combustion products for the S38 (closed symbols, —) and S50 (open symbols, – · –) flames.

ing reactions:

(1) In the fuel-rich zone the primary fuel degradation takes place with a net conversion of C_2H_2 through the following reaction:

$$C_2H_2 + H \leftrightarrow C_2H_3.$$

(2) In the partial oxidation zone that is identified by the oxidation of C_2H_2 into CO and the production of H_2, the following reactions are suggested:

$$C_2H_2 + O \leftrightarrow CH_2 + CO,$$

$$C_2H_2 + O \leftrightarrow HCCO + H,$$

$$C_2H_2 + OH \leftrightarrow HCC + H_2O,$$

$$C_2H_3 + O_2 \leftrightarrow CHO + CH_2O,$$

$$CH_2O + H \leftrightarrow CHO + H_2,$$

$$CHO + M \leftrightarrow CO + H + M.$$

(3) In the total oxidation zone, the formation of H_2O and conversion of CO to CO_2 occurs via

$$H_2 + OH \leftrightarrow H_2O + H,$$

$$CO + OH \leftrightarrow CO_2 + H.$$

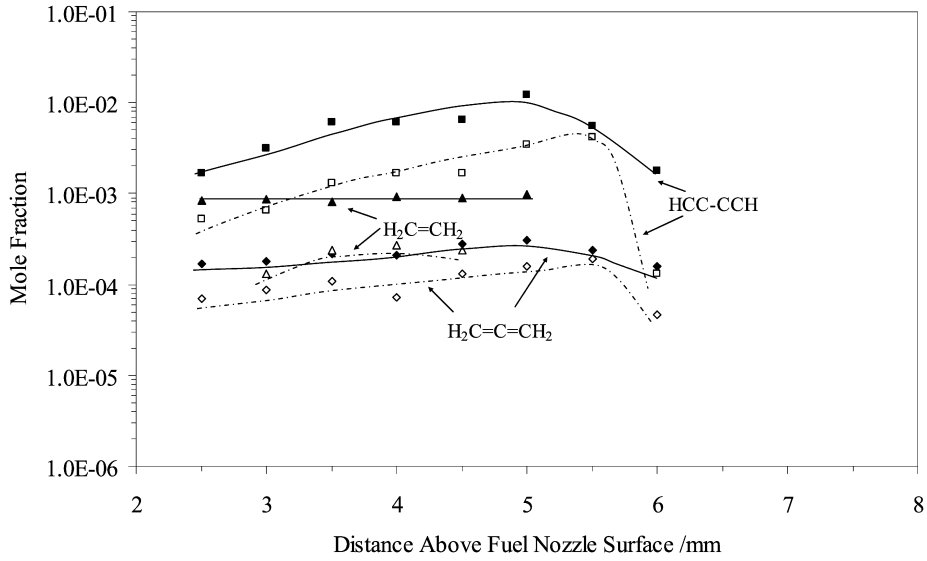

Fig. 7. Mole fraction profiles of aliphatic products for the S38 (closed symbols, —) and S50 (open symbols, – · –) flames.

In Fig. 7, the mole fraction profiles for some of the aliphatic combustion products, such as C_2H_4, HCC-CCH, and CH_2CCH_2, are presented for both flames. As evident from this figure, these trace hydrocarbon intermediates were produced within the fuel side of the flame and were subsequently destroyed at about 6.0–6.5 mm from the fuel burner surface through oxidation reactions. Similar behavior was also exhibited by all hydrocarbon by-products formed in these flames. It is particularly significant to note that the levels of these trace intermediates were substantially lower in the higher strain S50 flame than in the S38 flame. The peak concentrations and locations of HCC-CCH were 1×10^{-2} at 5.0 mm and 4×10^{-3} at 5.5 mm for the S38 and S50 flames, respectively, representing a factor of 2 difference. The mole fractions C_2H_4 and CH_2CCH_2 were not particularly sensitive to flame location. These intermediates were likely to be produced via the reactions

$$C_2H_3 + H_2 \leftrightarrow C_2H_4 + H,$$

$$HCC + CCH \leftrightarrow HCC\text{-}CCH,$$

$$C_2H_2 + CH_2 \leftrightarrow CH_2CCH_2.$$

Mole fraction profiles of aromatics by-products such as C_6H_6 (benzene) and $C_{10}H_8$ (naphthalene) are shown in Fig. 8. Again these incomplete combustion by-products were generated on the fuel side of the flame, and their levels were strongly dependent on the flame strain rate. The peak mole fractions of benzene and their flame positions were 2×10^{-4} at 5.0 mm and 8×10^{-5} at 5.0 mm for the S38 and S50 flames, respectively. Similarly, the peak mole fractions and locations for naphthalene in the S38 and S50 flames were 4×10^{-5} at 4.5 mm and 5×10^{-6} at 5.0 mm, respectively.

Several mechanisms have been proposed to describe the formation of benzene at elevated temperatures [6,11]. In one mechanism, the first aromatic ring forms by the addition of a vinylic radical (C_4H_3) to acetylene [6]:

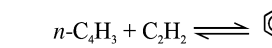

In another mechanism, benzene formation in flames was advocated to occur through the recombination of propargyl radicals [11]:

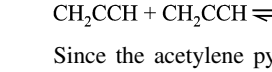

Since the acetylene pyrolysis products contain both even and odd number of carbon atoms (see Figs. 2 and 7), both routes can play a role in benzene formation in acetylene flames.

Naphthalene can then be formed through hydrogen abstraction from benzene followed by sequential acetylene addition reactions [6]:

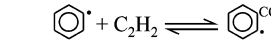

In addition, naphthalene has been proposed to form through recombination of the two cyclopentadienyl radicals, C_5H_5 [11]. Again the detection of by-products containing both even and odd numbers of carbon atoms suggests that both mechanisms can be at play in acetylene flames.

Mole fraction profiles of 3- and 4-ring aromatic products formed are shown in Fig. 9. It is interesting to note that for these PAH, their levels were most sensitive to the flame strain rate. For example,

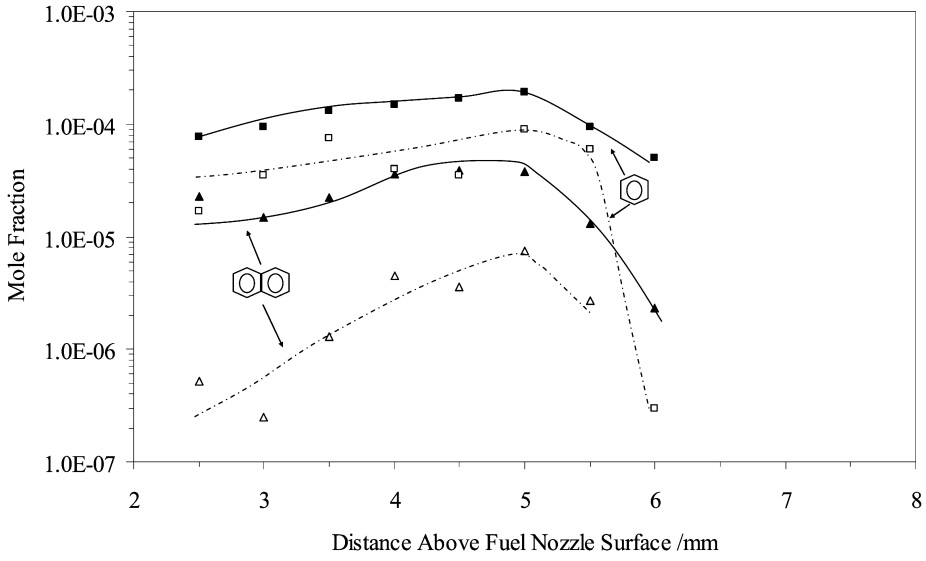

Fig. 8. Mole fraction profiles of single- and two-ring aromatic products for the S38 (closed symbols, —) and S50 (open symbols, – · –) flames.

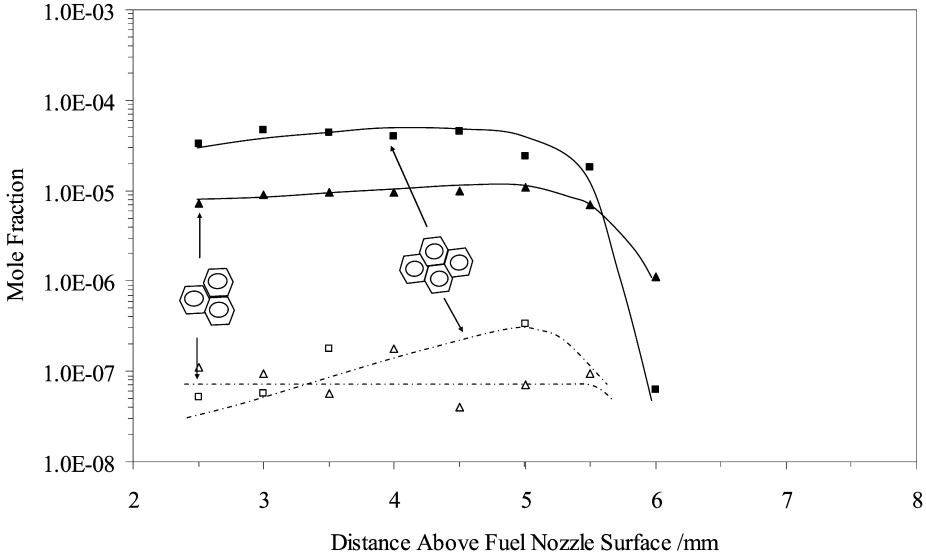

Fig. 9. Mole fraction profiles of three- and four-ring aromatic products for the S38 (closed symbols, —) and S50 (open symbols, – · –) flames.

the peak mole fraction profiles of $C_{14}H_{10}$ (phenanthrene) were 2×10^{-5} and 8×10^{-8} for the S38 and S50 flames, respectively, representing a two-order-of-magnitude difference. Similarly, the peak mole fractions of $C_{16}H_{10}$ (pyrene) were 3×10^{-5} and 4×10^{-7}, respectively, for flames S38 and S50, again representing a two-order-of-magnitude difference.

A variety of routes have also been proposed for the formation of phenanthrene [6,11]. For example, it can be produced from naphthalene by the sequential addition of two C_2H_3 moieties, or through the addition of C_2H_3 to biphenyl, the latter being produced by the addition of a phenyl radical to benzene. Similarly, pyrene can be produced by the direct addition of C_2H_3 to phenanthrene or by the sequential additions of 3 C_2H_3 moieties to naphthalene.

Clearly, the accurate identification of likely reaction pathways responsible for the formation and destruction of all the flame species discussed above can only be accomplished after a detailed chemical kinetic modeling exercise, which we hope our results will stimulate. Until this modeling work is completed, the

mechanistic comments made above should be considered tentative at best.

In summary, detailed chemical structures of counterflow acetylene flames determined at different strain rates reveal a number of significant results. First, strain rates do not significantly alter the major species concentration profiles in flames, suggesting that the major features of diffusion flames can be modeled relatively easily. On the other hand, the concentrations of high-molecular-weight trace hydrocarbon intermediates formed in diffusion flames were very strongly influenced by the strain rate. The latter necessitates the development of highly accurate detailed chemical kinetic mechanisms describing the formation and destruction of combustion by-products or intermediates.

Acknowledgment

This research was supported by the U.S. Environmental Protection Agency.

References

[1] N. Olten, S.M. Senkan, Combust. Sci. Technol. 159 (2000) 1–15.
[2] M.J. Castaldi, A.M. Vincitore, S.M. Senkan, Combust. Sci. Technol. 107 (1995) 1–19.
[3] A.M. Vincitore, S.M. Senkan, Combust. Sci. Technol. 130 (1997) 233–246.
[4] R. Barthel, S. Senkan, Combust. Sci. Technol. 101 (1994) 187.
[5] M. Qun, S. Senkan, Combust. Sci. Technol. 101 (1994) 103.
[6] M. Frenklach, D.W. Clary, W.C. Gardiner, S.E. Stein, Proc. Combust. Inst. 20 (1985) 887–896.
[7] R.P. Lindstedt, G. Skevis, Combust. Sci. Technol. 125 (1997) 73.
[8] H. Richter, J.B. Howard, Phys. Chem. Chem. Phys. 4 (2002) 2038.
[9] I. Glassman, Combustion, second ed., Academic Press, New York, 1987.
[10] K.K. Kuo, Principles of Combustion, Wiley, New York, 1986.
[11] N. Marinov, W.J. Pitz, C.K. Westbrook, A.M. Vincitore, M.J. Castaldi, S.M. Senkan, C.F. Melius, Combust. Flame 114 (1998) 192.
[12] S. Granata, T. Faravelli, E. Ranzi, N. Olten, S. Senkan, Combust. Flame 131 (2002) 273.
[13] J.P. Gore, S.M. Skinner, Combust. Flame 87 (1991) 357–364.
[14] J.P. Gore, U.S. Ip, Y.R. Sivathanu, J. Heat Transfer 114 (1992) 487–493.
[15] M. Saito, T. Arai, M. Arai, Combust. Flame 119 (1999) 356–366.
[16] A. Hamins, A.S. Gordon, K. Saito, K. Seshadri, Combust. Sci. Technol. 45 (1986) 309–310.
[17] C.J. Sun, C.J. Sung, H. Wang, C.K. Law, Combust. Flame 107 (1996) 321–335.
[18] K.C. Lin, P.B. Sunderland, G.M. Feath, Combust. Flame 104 (1996) 369–375.
[19] P.B. Sunderland, U.O. Koylu, G.M. Faeth, Combust. Flame 100 (1995) 310–322.
[20] N. Olten, S.M. Senkan, Combust. Flame 118 (1999) 500–507.
[21] A.M. Vincitore, S.M. Senkan, Combust. Flame 114 (1998) 259–266.
[22] J. Vandooren, P.J. Van Tiggelen, Proc. Combust. Inst. 16 (1976) 1133.
[23] P.R. Westmoreland, J.B. Howard, J.P. Longwel, Proc. Combust. Inst. 21 (1986) 773.
[24] P.B. Sunderland, U.O. Koylu, G.M. Faeth, Combust. Flame 105 (1996) 132–146.
[25] C.M. White, J. Chem. Eng. Data 31 (1986) 198.
[26] W.L. Fitch, A.D. Sauter, Anal. Chem. 55 (1983) 832.
[27] S.C. McEnally, L.D. Pfefferle, Combust. Flame 117 (1999) 362–372.
[28] K.W. Lee, M.S. thesis, UCLA, 1999.
[29] K. Seshadri, F.A. Williams, Int. J. Heat Mass Transfer 21 (1978) 251–253.
[30] M. Yamamato, M.S. thesis, Department of Chemical Engineering, University of California, Los Angeles, 2000.